



Quantification of oxygen isotope SIMS matrix effects in olivine samples: Correlation with sputter rate



J. Isa*, I.E. Kohl, M.-C. Liu, J.T. Wasson, E.D. Young, K.D. McKeegan

Department of Earth, Planetary, and Space Sciences, University of California, Los Angeles, United States

ABSTRACT

We investigated the magnitude and reproducibility of instrumental mass-dependent fractionation of oxygen isotopes in secondary ion mass spectrometry (SIMS) analyses of olivine crystals of different major element chemistry (from Mg-rich to Fe-rich) in order to improve the accuracy of in-situ O-isotope measurements in geochemical/cosmochemical olivine samples. We found that oxygen isotope SIMS matrix effects are reproducible, and developed a model curve that can be used for correcting instrumental mass fractionation of olivine samples of intermediate chemical composition. The changes in instrumental mass fractionations were likely caused by differing Cs concentrations in the near surface regions of the samples due to different sample sputtering rates.

1. Introduction

Secondary ion mass spectrometry (SIMS) is a useful technique for analyzing isotope abundances in cosmochemical and geochemical samples because of its excellent spatial resolution. For light elements ($m < \sim 60$ amu) with relatively high ionization yields, SIMS can provide high precision (sub-permil) analyses of isotope ratios. As with all mass spectrometers, instrumental biases (e.g., mass-dependent fractionations) are calibrated by the use of standard materials, thereby enabling isotope ratios to be reported on a conventional normalized scale (e.g., Standard Mean Ocean Water, SMOW, for oxygen or hydrogen isotopes). Problems can arise due to a lack of appropriate standard materials; such problems can be particularly acute for SIMS, limiting both precision and accuracy of isotopic analyses. Precision is, in part, dependent on the homogeneity of an isotopic standard at fine spatial scales, a characteristic that typically can be assessed only through repeated SIMS measurements. However, even after homogeneity of a material is established, its suitability as a standard for a given isotopic analysis depends on how well the material matches the mineralogical and chemical composition of the target sample(s). This is because elemental and isotopic fractionations in SIMS are inherent in the sputtering process and thus depend upon the interactions of the primary ion beam with the target material. Ionization yields of sputtered target atoms are a function of the near-surface chemical composition of the target and are generally $< 1\%$, even for sputtering with reactive primary ion beam species. Thus, instrumental fractionations can be discrepant for materials of differing chemical compositions

or crystallinity, leading to inaccurate analyses should an inappropriate standard be used for calibration. The resultant error is referred to as a “matrix effect” since it is generated by a mismatch between the matrix of the sample being analyzed and that of the standard used to calibrate instrumental fractionation.

In situ analysis of oxygen isotope abundances was recognized as an important early application of SIMS, and this continues to the present day. Accordingly, significant efforts have been made to develop standard materials and to quantify matrix effects on SIMS oxygen isotope measurements. The most comprehensive work has involved oxygen isotope analyses of various silicate minerals made under energy filtering with selection of high-energy secondary ions (Eiler et al., 1997; Riciputi et al., 1998). This approach was taken in the hope that, by analyzing only secondary ions that were sputtered from a sample with high initial kinetic energy (typically > 325 eV), matrix effects would be reduced and/or instrumental mass fractionation (IMF) would be more stable and could be modeled by systematic parameterization(s). These early investigations demonstrated some general trends between IMF and sample characteristics, for example mean atomic mass. Among related minerals, the IMF was found to correlate with simple chemical parameters; for example, within the olivine solid-solution series the magnitude of oxygen isotope IMF increased linearly with forsterite content by approximately $6\%/amu$ over a range of ~ 0.2 in molar Mg/(Mg + Fe) content (Eiler et al., 1997; Riciputi et al., 1998). Interpolation over this limited range in olivine chemistry permitted analytical accuracy in $\delta^{18}O$ of $\sim 1\%$, which was commensurate with the precision obtained with this method that utilized magnetic field peak-hopping

* Corresponding author.

E-mail address: jisa@ucla.edu (J. Isa).

and ion counting with electron multipliers. However, extrapolation to more Fe-rich compositions showed very large deviations from the linear relationship, resulting in a $\delta^{18}\text{O}$ error (matrix effect) ranging up to $\sim 20\%$ for pure fayalite (Eiler et al., 1997).

With the development of large-radius, forward-geometry ion microprobes (e.g., the CAMECA ims-1270 and -1280), rapid, high-precision ($< 0.5\%$) oxygen isotope measurements became possible by measuring isotope beams simultaneously with Faraday cup detectors distributed along the instrument's mass focal plane (e.g., Kita et al., 2009; Kolodny et al., 2003; Treble et al., 2007). To achieve the necessary high intensity signals from small ($\sim 10\text{--}25\ \mu\text{m}$) analytical spots, the mass spectrometer must be set to transmit the abundant, low-energy secondary ions, i.e., the peak of the sputtered ion energy distribution. These methods have supplanted the high energy-filtering approach because they enable much faster analyses (3–5 min vs. 15–30 min) that consume less sample while still yielding significantly improved precision. However, higher precision without an equivalent increase in accuracy is always problematic, and therefore today's analyses also require an improved quantification of matrix effects appropriate to the analytical conditions utilized.

In this contribution, we focus on oxygen isotope analyses of olivine. We are interested in meteoritic samples that often span a very wide range in FeO contents compared to terrestrial mantle olivines (Criss, 2008 and references therein); for example, olivine phenocrysts in unequilibrated carbonaceous chondrites range from $\sim\text{Fa}0$ to $\text{Fa}80$ (e.g., Wasson and Rubin, 2003), olivine in martian meteorites is intermediate from $\sim\text{Fa}20$ to $\text{Fa}50$ (e.g., Mikouchi et al., 2001), olivine in HED meteorites is $\sim\text{Fa}30$ to $\text{Fa}90$ (Warren et al., 2014 and references therein), and olivine in angrites goes from $\sim\text{Fa}10$ to $\text{Fa}86$ (Keil, 2012). Previous studies of matrix effects in meteoritic olivine have come to different conclusions. Valley and Kita (2009) found significant matrix effects that varied non-linearly from forsterite to fayalite, however only a limited number of intermediate composition olivines were investigated with no samples analyzed between $\text{Fa}40$ and $\text{Fa}100$. In contrast, Jogo et al. (2012), using similar analytical methods and instrumentation, found no systematic differences in IMF among terrestrial ($\text{Fa}11$) and meteoritic ($\text{Fa}35$ and $\text{Fa}63$) olivine standards. The reasons for this discrepancy are not apparent.

Our goal here is to investigate oxygen isotope IMF over the entire olivine Fe-Mg solid-solution series. We determined the oxygen isotope compositions of nine separate, homogeneous olivine samples by laser-assisted fluorination isotope-ratio mass spectrometry and then made high precision SIMS analyses of the same samples to define a calibration curve between instrumental mass fractionation and sample compositions. We also investigated whether matrix effects correlate with the concentration of Cs ions implanted in the sample surface. Our results permit interpolation of matrix effects for intermediate olivines, thereby enabling high precision and high accuracy for investigations of cosmochemical samples.

1.1. Sample and analytical technique

Seven terrestrial and two meteoritic olivine samples, covering a wide range of Fe/Mg compositions, were studied (Table 1). The sample descriptions are in the appendix. All samples were handpicked under a binocular microscope. The samples were carefully examined to avoid other phases such as opaque inclusions, or yellow brown to dark brown colored veins that probably consisted of carbonate and Fe-bearing oxide. Some grains were mounted in epoxy resin or indium for SIMS measurements, while other portions of selected grains were used for laser fluorination analysis. Several samples (Day Book dunite, Rockport, and those from the Skaergaard intrusion) were washed prior to laser fluorination analysis to dissolve adhering opaque oxides and other weathering materials. The samples were washed in individual beakers by following a protocol of hydrochloric acid (3 mol/l overnight), deionized water in an ultrasonic bath, nitric acid (2 mol/l overnight), deionized water in an ultrasonic bath, and methanol in an ultrasonic bath. After the acid treatment, the samples looked transparent and had a uniform color (yellow to slightly green in the range $\text{Fa}0$ to $\text{Fa}70$). All samples were dried in an oven at $50\ ^\circ\text{C}$ for three to five days prior to the laser fluorination analysis.

Quantitative mineral elemental compositions were obtained by electron microprobe analysis (EPMA) with the UCLA JEOL8200, with 20 s counting times for peaks and 5 s counting time for backgrounds. The beam currents used were $\sim 15\ \text{nA}$ at 15 kV; ZAF corrections were made.

For laser-assisted fluorination, samples were melted in the presence of fluorine gas by irradiation with an infrared laser and the isotopic composition of liberated oxygen was measured with a Thermo Finnigan Delta Plus gas-source isotope ratio mass spectrometer (IRMS) in Dual Inlet mode at the Stable Isotope Lab, UCLA, following methods most recently described in Young et al. (2016). SIMS analyses were performed on the UCLA 1270 and 1290 ion microprobes by using a primary Cs^+ beam and analyzing low-energy (0–25 eV) negative secondary ions. The measurements were carried out during four different analytical sessions, with the ims-1270 in 2012, 2013 and 2014, and with the ims-1290 in 2017. On the ims-1270, samples were sputtered with a 20 keV Cs^+ primary beam with intensities of 3, 4 and 6 nA focused to spots with a diameter in the range of 20–40 μm ; on the ims-1290, primary beam intensities of 2.5 nA and 4 nA were used (spot sizes $\sim 10\text{--}20\ \mu\text{m}$). A normal incidence electron gun was used to compensate for sample charging. Oxygen isotopes ^{16}O and ^{18}O were measured simultaneously by using two Faraday cups (10^{10} and $10^{11}\ \Omega$ resistors) in the multicollection system. The acquisition times per analysis spot on the ims-1270 were 200 s (12 to 15 cycles of 10 s integration) and resulted in internal uncertainties $< 0.1\%$. On the ims-1290, secondary ions were counted for $\sim 1\ \text{min}$ (10 cycles of 5 s integrations) and internal and external uncertainties between 0.1% and 0.2% were achieved. The relative sputter rates for individual

Table 1
Olivine standard materials used in this study.

Name of sample	Fa	Locality	Source and sample identifier
Pine River IAB iron meteorite	2	N/A	UCLA, IN 314
Day Book dunite	7	Yancey County, North Carolina, USA	NMNH 119138
Mt. Franklin	8	Victoria, Australia	Paul Warren (UCLA)
San Carlos	9	San Carlos, Gila County, Arizona, USA	Christopher Snead (UCLA)
Urals	16	Lake Itkul, Sverdlovsk, Urals, Russia	NMNH 16257-01
Skaergaard EG 5108	35	Skaergaard Intrusion, East Greenland	Oxford U., EG5108
NWA 6693 achondrite	50	N/A	UCLA, LC 2617 and LC 2618
Skaergaard EG 1907	69	Skaergaard Intrusion, East Greenland	Oxford U., EG1907
Rockport	97	Essex County, Massachusetts, USA	NMNH 85276

samples were calculated based on the depths of crater pits sputtered in a 50 $\mu\text{m} \times 50 \mu\text{m}$ raster mode with a 5 nA primary Cs^+ beam by ims-1270. Each sample was sputtered for 20 min. The crater pits depths were measured with a MicroXam interferometer.

For each SIMS analytical session, measurements of San Carlos olivine (hereafter, SC-olivine) were used to calibrate the instrumental mass fractionation and the relative yields of the two Faraday cup detectors used for the $^{18}\text{O}^-$ and $^{16}\text{O}^-$ beams. Although Faraday cup amplifier gains are calibrated electronically at the outset of each analysis session, this intercalibration is not necessarily accurate at the permil level. This is acceptable because the relative amplifier gains are stable on the time scale of an analytical session (typically 1 day) and thus the overall calibration is reliant on the reproducibility of analyses of the primary standard (SC-olivine). We thus define the overall correction factor as “instrumental mass fractionation” (IMF) according to:

$$\text{IMF} = (^{18}\text{O}/^{16}\text{O})_{\text{SC-SIMS}} / (^{18}\text{O}/^{16}\text{O})_{\text{SC-LF}} \quad (1)$$

where $(^{18}\text{O}/^{16}\text{O})_{\text{SC-SIMS}}$ refers to the isotopic ratio in SC-olivine measured by SIMS and $(^{18}\text{O}/^{16}\text{O})_{\text{SC-LF}}$ is the “true” value determined by laser-fluorination ($\delta^{18}\text{O}_{\text{SMOW}} = 5.19\text{‰}$). In the absence of matrix effects, the measured $^{18}\text{O}/^{16}\text{O}$ ratios of other olivine grains can be corrected for IMF obtained in each session by:

$$(^{18}\text{O}/^{16}\text{O})_{\text{SIMS,corrected}} = (^{18}\text{O}/^{16}\text{O})_{\text{SIMS,measured}} / \text{IMF} \quad (2)$$

The ratios can then be converted to delta-notation by normalizing to the accepted value of $^{18}\text{O}/^{16}\text{O}$ in standard mean ocean water ($(^{18}\text{O}/^{16}\text{O})_{\text{SMOW}} = 0.00200520$; Baertschi, 1976):

$$\delta^{18}\text{O} = [(^{18}\text{O}/^{16}\text{O})_{\text{SIMS-corrected}} / (^{18}\text{O}/^{16}\text{O})_{\text{SMOW}} - 1] \times 1000 \quad (3)$$

The $\delta^{18}\text{O}$ values of all olivine standards measured in this study by laser-assisted fluorination are given in Table 3. The corresponding oxygen isotope ratios of these olivines can be calculated via:

$$(^{18}\text{O}/^{16}\text{O})_{\text{LF}} = [\delta^{18}\text{O}/1000 + 1] \times (^{18}\text{O}/^{16}\text{O})_{\text{SMOW}} \quad (4)$$

The gas-source Isotope Ratio Mass Spectrometry (IRMS) analyses are calibrated by sample standard bracketing with a reference gas, thus if the laser-assisted fluorination reactions go perfectly to completion (producing purified O_2 gas), analyses are free of matrix effects. Said another way, with 100% yield the gas in an IRMS measurement perfectly reflects the isotope ratio and molar amount of analyte contained within the starting material. Repeated measurements of San Carlos olivine in the UCLA IRMS laboratory coinciding with this study yielded results, precise and accurate at the level of $\pm 0.13\text{‰}$ 1 S.D. or $\pm 0.033\text{‰}$ at 1 standard error of the mean ($n = 17$) (Young et al., 2016).

2. Results

The chemical compositions of the olivines investigated are given in Table 2 as the average of replicated electron microprobe analyses. Compositions range from very magnesian (Fa2) to nearly pure fayalite, with 4 samples spanning intermediate compositions between San Carlos (Fa9) and the Rockport end-member (Fa97). All samples are close to the forsterite-fayalite join, with only minor amounts of elements other than Mg, Fe, Si and O. Only the Rockport sample has an appreciable tephroite component, with 2.2 wt% MnO, and the Skaergaard samples EG 5108 and EG1907 are the only others to have detectable MnO at ~ 0.4 and ~ 0.8 wt%, respectively. Fayalite content is calculated as mol % $\text{Fe}/(\text{Mg} + \text{Mn} + \text{Fe})$; estimated uncertainties in the reported fayalite compositions are $\sim 0.1\%$ to 0.7% .

The IMF-corrected $\delta^{18}\text{O}$ values on the SMOW-scale are given in Table 4. Repeated measurements of San Carlos olivine yielded an external reproducibility of $\pm 0.2\text{‰}$ 1 S.D. ($n = 77$). It is readily observed (Fig. 1) that the SIMS $\delta^{18}\text{O}$ values (calculated by Eq. (3) and listed in Table 4) do not agree in all cases with the values

determined by laser-fluorination (Table 3); the discrepancies are attributed to SIMS matrix effects.

The magnitude of the SIMS matrix effect for a given sample is calculated as the difference, expressed in permil, between the instrumental fractionation determined on a sample compared to that determined for the primary standard, San Carlos olivine, under the same experimental conditions. Thus, matrix effect is quantified by the expression:

$$1000 (\ln(\alpha) - \ln(\text{IMF})),$$

where $\alpha = (^{18}\text{O}/^{16}\text{O})_{\text{SIMS}} / (^{18}\text{O}/^{16}\text{O})_{\text{LF}}$ (5)

and IMF is defined for each analytical session by Eq. (1). These matrix effects vary with olivine composition: they are relatively small to unresolvable within our experimental uncertainties among Mg-rich olivines ($\text{Fa} < 25$), but they increase in magnitude with increasing Fe content, reaching values of -6 to -11‰ for Fe-rich olivines ($\text{Fa} > 95$) under our experimental conditions.

Relative sputter rates were determined for each olivine composition by measuring the crater depth resulting from sputtering by a ~ 5 nA Cs beam rastered over $50 \times 50 \mu\text{m}$ for 20 min. The measured depths are normalized for small deviations in primary beam intensity from the intended 5 nA current (Table 5). The reported uncertainty in the calculated relative sputter rates is taken as the reproducibility of crater depths for repeated sputtering experiments on San Carlos olivine in different mounts.

3. Discussion

The primary goal of this work was to determine if systematic behavior of the SIMS IMF could be found such that precise and accurate measurements of oxygen isotopes for olivine of intermediate Fa content could be “routinely” achieved with an appropriate calibration for matrix effects. A fundamental requirement for this to be useful in a practical sense is that the matrix effect systematics be reproducible, at least over instrumental conditions that are sufficiently well-defined as to be routinely achievable. As can be seen in Table 4, analyses made years apart for five olivine samples (in addition to the primary standard, San Carlos) with two SIMS instruments yielded reproducible results within experimental uncertainties of typically a few tenths permil for all the samples except “Day Book dunite” and “Rockport”. For example, analyses of olivine EG 5108 Skaergaard with composition Fa34 agreed within 0.1‰, allowing for precise calibration of a small matrix effect of -0.6‰ (relative to San Carlos). The Day Book dunite olivine Fa values are similar to that of San Carlos olivine, and therefore any matrix effect is expected to be small. Instead, a relatively large dispersion of the data was found, and this is likely attributable to the sample heterogeneity. We therefore excluded Day Book dunite olivine from further consideration as a standard suitable to calibrate matrix effects.

For the Rockport olivine, a nearly pure fayalite end-member, multiple SIMS analyses performed on the ims-1270 in 2013 and 2014 produced San Carlos normalized $\delta^{18}\text{O}$ values that disagreed by up to 3‰ (Table 4) suggesting either sample heterogeneity or irreproducibility in calibrating the matrix effect at this extreme iron content. Following a suggestion by Noriko Kita, we found that the dispersion in the data was associated with the primary beam intensity used in the analysis, which ranged from ~ 3 nA to ~ 6 nA in different analytical sessions (Fig. 2b). Such an effect is unexpected based on sputtering theory, so to investigate further we made a series of measurements with different Cs + beam currents, this time using the ims-1290. Because a 6 nA Cs + beam yielded $^{16}\text{O}^-$ signals that were too high, saturating the FC amplifier ($10^{10} \Omega$ resistor), we proceeded with the measurements using beams of 4.2 nA down to 2.5 nA. Charge compensation was achieved by a normal incidence electron gun, as in the previous experiments. However, this time we found no evidence for any

Table 2
Chemical compositions of olivine samples (wt%).

	Pine River		Day Book dunite		Mt. Franklin		San Carlos	Urals	
	Average n = 5	std.	Average n = 3	std.	Average n = 3	std.	Average n = 2	Average n = 3	std.
SiO ₂	41.5	0.6	41.3	0.2	41.2	0.2	41.0	39.71	0.02
TiO ₂	–	–	< 0.04	–	< 0.04	–	< 0.04	< 0.04	–
Al ₂ O ₃	< 0.04	–	< 0.04	–	< 0.04	–	< 0.04	< 0.04	–
Cr ₂ O ₃	< 0.04	–	< 0.04	–	< 0.04	–	< 0.04	< 0.04	–
MgO	54.9	0.8	51.2	0.1	50.6	0.1	49.7	44.6	0.1
CaO	< 0.04	–	< 0.04	–	0.08	0.01	0.09	< 0.04	–
FeO	2.0	0.7	7.3	0.1	7.9	0.2	8.6	15.3	0.1
MnO	0.20	0.04	0.13	0.03	0.09	0.02	0.13	0.17	0.01
NiO	–	–	0.4	0.1	0.42	0.04	0.36	0.33	0.04
Total	98.6		100.2		100.2		99.8	100.2	
Fa mol%	2.0		7.4		8.0		8.8	16.1	

	Skaergaard EG 5108		NWA6693		Skaergaard EG1907		Rockport	
	Average n = 3	std.	Average n = 17	std.	Average n = 6	std.	Average n = 15	std.
SiO ₂	37.1	0.1	35.2	0.2	33.2	0.2	29.9	0.3
TiO ₂	< 0.04	–	–	–	–	–	–	–
Al ₂ O ₃	0.05	0.03	–	–	–	–	–	–
Cr ₂ O ₃	< 0.04	–	–	–	–	–	–	–
MgO	32.4	0.1	23.2	0.2	13.4	0.2	0.10	0.03
CaO	0.06	0.02	0.09	0.03	0.09	0.02	0.08	0.02
FeO	31.09	0.04	41.9	0.3	53.9	0.2	67.8	0.2
MnO	0.43	0.03	0.29	0.02	0.79	0.02	2.2	0.1
NiO	0.12	0.03	–	–	–	–	–	–
Total	101.3		100.7		101.4		100.0	
Fa mol%	34.8		50.2		68.6		96.6	

Fa mol% = Fe / (Mg + Mn + Fe) × 100. std.: a standard deviation (%).

correlation of IMF with primary beam intensity (Fig. 2a). The matrix effect between Rockport and San Carlos was a constant – 9.3‰ over a dozen spots analyzed. We conclude that the apparent primary beam dependent matrix effects seen earlier were the result of improper charge compensation on very Fe-rich olivine under the relatively high primary beam currents used previously. The fact that this artifact only became apparent for the most Fe-rich sample makes sense because the charging condition in the analysis spot can be different for samples of differing conductivity if the electron cloud produced by the normal incidence electron gun is not tuned properly, thus producing insufficient density above the sample surface to neutralize all buildup of positive charge. In such a case, the sample high voltage supply may provide more or less negative charge depending on primary beam current and surface conductivity, which would lead to a shift in the energy spectrum of the sputtered ions, thus changing the IMF. This experience underscores the need to be very cautious, for example by exploring a range of instrumental parameters, when attempting to calibrate mass fractionation of oxygen in very Fe-rich samples (especially if Fe-poor San Carlos olivine is used as a primary standard). In the remainder of this discussion analyzing systematic behavior of IMF, we consider only those data for Rockport that showed a constant matrix effect, independent of primary beam current.

The oxygen isotope matrix effects reported by various investigators utilizing different instruments and analytical approaches are shown as a function of olivine sample composition in Fig. 3a. The plot incorporates data obtained via Extreme Energy Filtering (EEF, Eiler et al., 1997; Riciputi et al., 1998) as well as data measured for low-energy secondary ions (Kita et al., 2010; Nakashima et al., 2013; Tenner et al., 2013, 2015; Valley and Kita, 2009) as was done in our study. As alluded to earlier, there is a wide variability in matrix effect behavior which depends strongly on the energy regime of the secondary ions analyzed. The magnitude of the matrix effect is in general much higher for

analyses made via EEF, which is perhaps not surprising given that the overall magnitude of the IMF is also much higher for very high energy secondary ions.

The good reproducibility of the matrix effects that we observe for the analyses of low energy secondary ions allows us to define a systematic behavior, dependent only on the Fa content of the olivine, that is sufficiently precise to allow for interpolation to derive IMF for an olivine of intermediate composition for which a standard of closely matching Fe-content is unavailable (Fig. 3b). The empirical correction curve can be fit by either a sigmoid or a quadratic expression where the matrix effect relative to San Carlos olivine is given by $-87.8 / (1 + \exp(2.14 \times (100 / \text{Fa})))$ or $-10.6 \times p^2$ with $p = (\text{Fa} / 100 - 0.09)$, respectively. Note that SC-olivine Fe molar fraction is 0.09. The scatter about the calibration curve is shown as a function of Fa content in Fig. 3c; the residual errors are characterized by a standard deviation of 0.4‰, which is a measure of the overall accuracy in $\delta^{18}\text{O}$ over the Fo-Fa solid solution.

In principle, our empirical correction curve could be instrument-dependent. However, the fact that our data from both ims-1270 and ims-1290 plot within error of the model curve indicates that matrix effects measured for low-energy secondary ions are similar, regardless of the instrument used. As can be seen in Fig. 3b, this expectation is confirmed by examining olivine O-isotope data from other studies measuring low-energy ions (Kita et al., 2010; Nakashima et al., 2013; Tenner et al., 2015, 2013; Valley and Kita, 2009). Additional complications could arise due to the orientation of crystal faces relative to the sputtering beam which is thought to play a role in causing small variability in IMF for SIMS oxygen isotope measurements of Fe-oxides (Huberty et al., 2010). Although such effects have not been demonstrated in silicates, we minimized the possibility of systematic shifts due to crystallographic orientation by analyzing multiple grains at random orientations. The good agreement of our data, obtained over multiple

Table 3
 $\delta^{18}\text{O}$ values measured by the laser-assisted fluorination technique.

Name	Fa	$\delta^{18}\text{O}$	Error ^a
Day Book dunite	7	5.61	0.13
Mt. Franklin	8	4.92	0.14
San Carlos	9	5.19	0.13
Urals	16	6.33	0.13
Skaergaard EG 5108	35	4.54	0.14
NWA 6693	50	3.86	0.13
Skaergaard EG 1907	69	4.28	0.13
Rock Port	97	4.74	0.14
Pine River ^b	2	4.48	

^a Error (%) = $\sqrt{(SD)^2 + (SE)^2}$.
^b Clayton and Mayeda (1986).

analytical sessions, with data obtained under generally similar experimental conditions but in a different laboratory (Kita et al., 2010; Nakashima et al., 2013; Tenner et al., 2013, 2015; Valley and Kita, 2009) demonstrates that the major cause of matrix effects in the olivine solid-solution series is the Fa content and that SIMS IMF can be corrected empirically with an accuracy that is close to analytical precision.

3.1. Relationship to sputter rate

The fit shown in Fig. 3b is purely empirical and the question arises whether there is some underlying physical reason for the dependence of oxygen isotope IMF on Fe concentrations in olivine. In the course of our investigations, we found that the sputter rate of olivine also varies systematically with Fe-content (Fig. 4). For a given beam current, impact energy, focusing condition, etc., fayalite sputters more quickly than does forsterite. This is important because the ionization yield of negative secondary ions (like O^-) is a strong function of the concentra-

Table 4
 $\delta^{18}\text{O}$ values measured by SIMS. The isotope ratios are normalized to San Carlos olivine ($\delta^{18}\text{O} = 5.2$) in each session.

Name	IMS-1270								
	2012 April			2013 May			2014 April		
	$\delta^{18}\text{O}$	std.	n	$\delta^{18}\text{O}$	std.	n	$\delta^{18}\text{O}$	std.	n
Pine River				4.6	0.3	5			
Day Book dunite	5.4	0.3	3	6.0	1.0	14			
Mt. Franklin	4.7	0.2	3	5.3	0.1	6			
San Carlos	≈ 5.2	0.2	5	≈ 5.2	0.3	31	≈ 5.2	0.2	10
Urals	6.0	0.1	3	6.3	0.3	11			
Skaergaard EG 5108	3.9	0.1	3	3.9	0.4	10			
NWA6693							2.6	0.2	11
Skaergaard EG 1907							1.1	0.2	11
Rock Port	-4.4	0.6	3	-6.4	0.4	15	-3.4	0.1	6

Name	IMS-1290		
	2017 Feb		
	$\delta^{18}\text{O}$	std.	n
Pine River	3.9	0.3	3
Day Book dunite			
Mt. Franklin	5.3	0.1	5
San Carlos	≈ 5.2	0.2	31
Urals	6.5	0.1	5
Skaergaard EG 5108	4.0	0.1	5
NWA6693	2.4	0.2	6
Skaergaard EG 1907	0.3	0.1	6
Rock Port	-4.3	0.3	12

n: number of analyses. std.: a standard deviation (%).

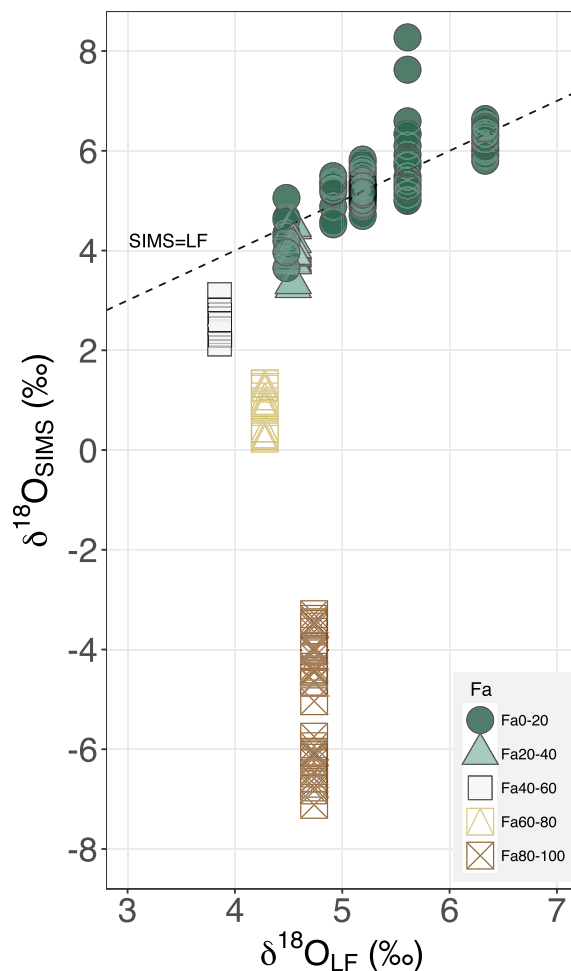


Fig. 1. $\delta^{18}\text{O}$ values of olivine samples measured by SIMS (data as acquired from individual SIMS spots) are plotted as a function of the true $\delta^{18}\text{O}$ as determined by laser fluorination (LF). Data are corrected for instrumental mass fractionation during SIMS analyses by comparison with San Carlos olivine (see text). The dashed 1:1 line represents where corrected $\delta^{18}\text{O}$ measured by SIMS and LF analyses agree; deviations from the line indicate matrix effects in the SIMS measurements. Fe concentrations of individual olivine are indicated in the legend: Fa = Fe/(Mg + Mn + Fe) mol%.

tion of Cs within the near surface of the sputtered area on the sample (e.g., Andersen, 1970; Yu, 1986). At steady-state, the concentration of Cs implanted from the primary ion beam is inversely proportional to sputter rate, so we might also expect that ionization yield would show a

Table 5
 Depth of SIMS crater after 20 min of sputtering under $50\ \mu\text{m} \times 50\ \mu\text{m}$ raster modes.

Name	Fa	Depth (nm)	I (nA)	5 nA normalized depth (nm)
Pine River IAB iron meteorite	2	360	5.1	360
Day Book dunite	7	400	5.2	380
Mt. Franklin	8	440	5.2	420
San Carlos	9	440	5.3	420
San Carlos	9	390	5.2	370
San Carlos	9	350	5.1	340
San Carlos	9	250	5.1	250
Urals	16	400	5.1	400
Skaergaard EG 5108	35	450	5.1	450
NWA 6693 achondrite	50	460	5.0	460
Skaergaard EG 1907	69	610	5.3	580
Rockport	97	710	5.2	690

I: primary beam intensity. Normalized depth: measured depth scaled to 5 nA primary beam intensity.

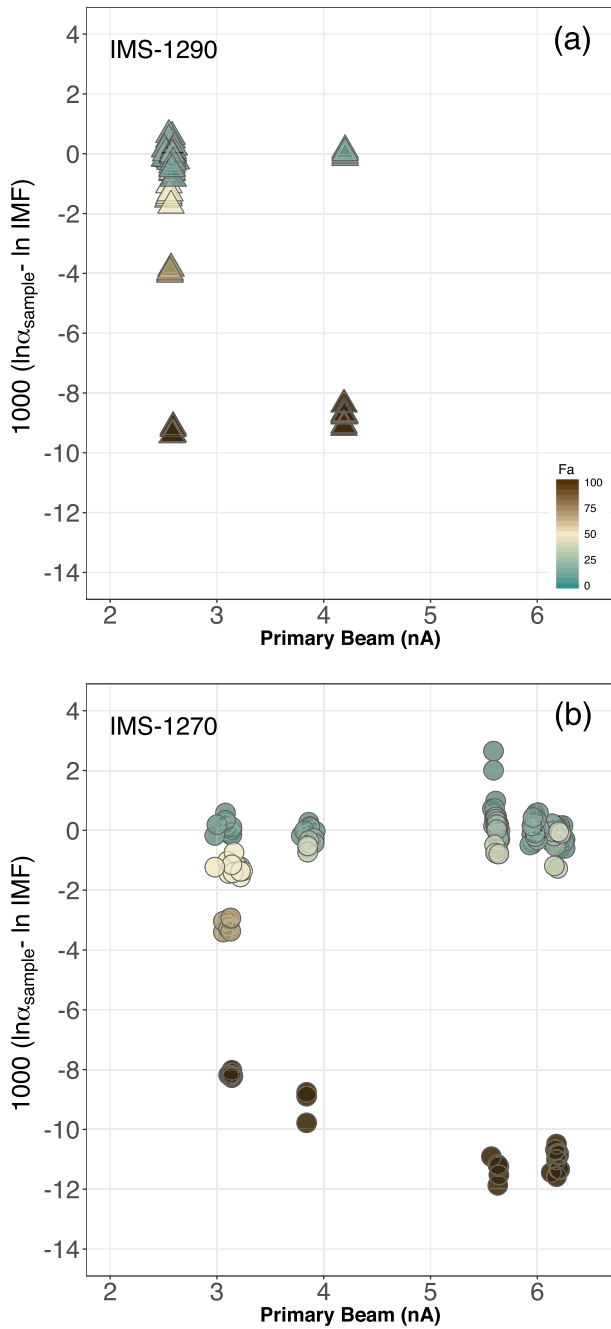


Fig. 2. O-isotope SIMS matrix effects for different primary beam intensities. The Fe molar fractions are expressed as $Fa = Fe / (Mg + Mn + Fe)$ mol% and color-coded. No primary beam effects were found among ims-1290 analyses (a), whereas data from measurements with ims-1270 indicate primary beam dependent matrix effects in Fe-rich samples (b) (see text). During a given analytical session, fluctuations of primary beam intensities are small.

dependence on sputter rate. For Cs bombardment of simple matrices (metals and metal silicides), Deline et al. (1978) found a non-linear relationship between negative ion useful yield (defined as number of ions detected/number of atoms sputtered) and inverse sputtering rate. Using Auger spectroscopy, Chelgren and colleagues quantified the measured surface Cs atom fraction and the useful yield of Si^- which varied by a factor of several thousand between Pt_2Si and Si metal (Chelgren et al., 1979). Although these studies were conducted to quantify matrix effects in the yield of negative ions for elemental analysis, similar principles must also apply to isotopic measurements, i.e., to SIMS IMF. The reasoning can be seen clearly by considering the limiting case: as useful yield approaches unity, instrumental mass

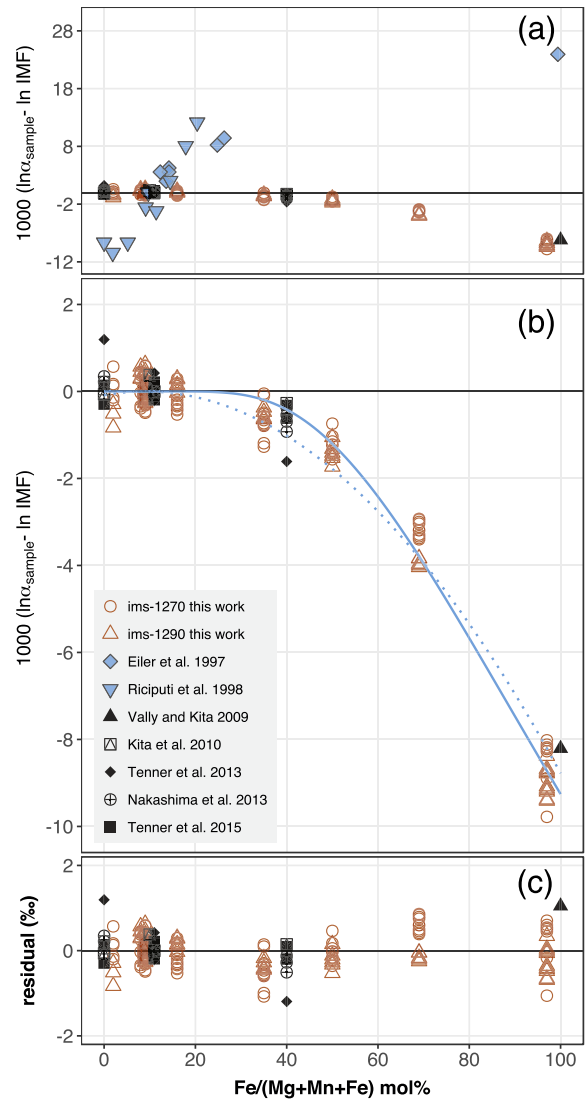


Fig. 3. O-isotope SIMS matrix effect as a function of Fe molar fractions of olivine. The Fe molar fractions are expressed as $Fe / (Fe + Mg + Mn)$ mol%. (a) Plotted are SIMS matrix effects normalized to SC-olivine (this study; also Valley and Kita, 2009; Kita et al., 2010; Tenner et al., 2013 and 2015; Nakashima et al., 2013) and extreme energy filtering results (Eiler et al., 1997; Riciputi et al., 1998) which are highlighted in blue. (b) SIMS matrix effect (excluding extreme energy filtering data) are fit by a sigmoidal curve, $y = -87.8 / (1 + \exp(2.14 \times (100 / Fa)))$ (blue solid line). The data can also be fit by a parabola $y = -10.6 \times p^2$ with $p = (Fa / 100 - 0.09)$ (blue dash line). (c) The residuals from the best regression curve (sigmoid) as a function of Fa content. The SIMS analytical reproducibility (a standard deviation of duplicated San Carlos olivine analyses) is 0.2‰ ($n = 77$). Most of the data from literature agree within 2 sigma of the fit curve. (For interpretation of the references to color in this figure legend, the reader is referred to the web version of this article.)

fractionation must go to zero, and if IMF is zero, then matrix effects vanish.

We did not directly measure absolute useful yields in this study, however a correlation of useful yield with matrix effect can be inferred from our data. As can be seen in Fig. 4, the sputter rate of Rockport is approximately 2 times faster than that of SC-olivine and therefore one would expect that the secondary ion intensity of oxygen from Rockport should be nearly double of that of SC-olivine (per nA Cs + bombardment). However, $^{16}O^-$ count rates of Rockport increased by only approximately 10 to 20% compared to that of SC-olivine, thus indicating that ionization yields of O^- are lower in fayalite than in Mg-rich olivine.

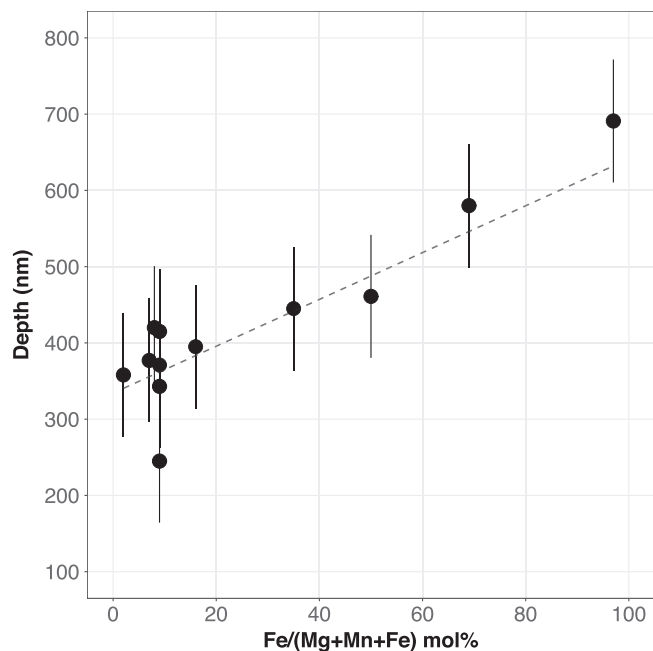


Fig. 4. Sputtered crater depth vs. molar fraction of Fe in olivine samples sputtered under fixed conditions. Relative sputter rate (proportional to the depth of the crater) is linearly correlated with the molar fraction of Fe in olivine.

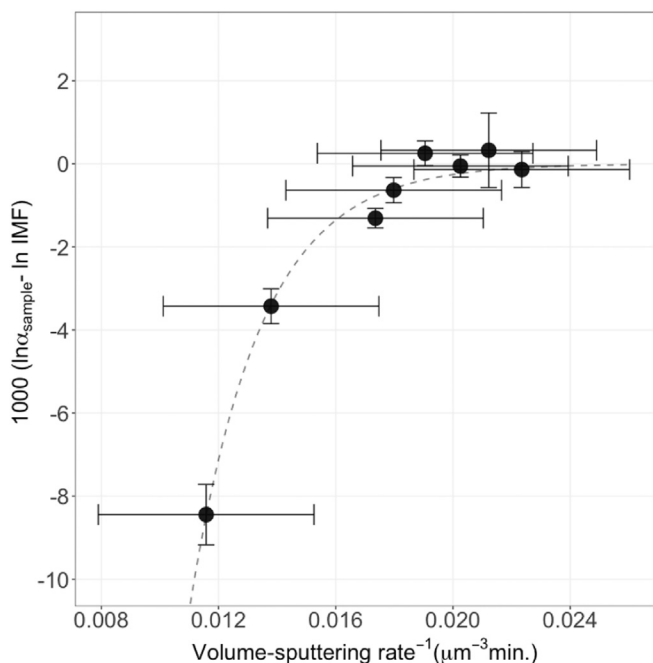


Fig. 5. Inverse of volume-sputtering rate vs. O-isotope SIMS matrix effect. The y-axis uncertainties are propagated errors based on the standard deviation of duplicated measurements for individual samples analyzed with IMS-1270 or IMS-1290, and a standard deviation of that for SC-olivine of 0.2‰ (n = 77). The SIMS matrix effect is correlated with the inverse sputtering rate which is proportional to the Cs⁺ concentration in the near surface of the sputtered sample (Deline et al., 1978). The regression curve is a sigmoid (see text).

We find that in olivine, O-isotope SIMS matrix effects are inversely correlated with sputter rate according to a sigmoid curve (Fig. 5). This is explained as a result of the difference in useful yield of O⁻ between Mg-rich and Fe-rich olivine, which is largely due to the difference in Cs concentration at the surface of the sputtered area. Fayalitic olivine, with its relatively high sputter rate, has a correspondingly low concentration of Cs and thus a relatively lower ionization for O⁻ and

therefore a larger instrumental mass fractionation. The nonlinear dependence of ionization probability on Cs concentration (Chelgren et al., 1979) results in a high sensitivity of the matrix effect for Fe-rich olivine. On the other hand, for sufficiently slow sputter rates (as in Mg-rich olivine), a threshold Cs concentration is achieved such that matrix effects become relatively insensitive to small changes in sputter rate due to changing Fa content. The phenomenon of Cs concentration reaching an effective saturation level for low sputter rates is consistent with a sigmoid curve as shown in Fig. 5.

The correlation of matrix effect with sputter rate, effectively a correlation with Cs concentration, is clear in a simple, essentially binary, solid solution series as in olivine. However, it is not straightforward to generalize this result to other mineral systems. For example, Page et al. (2010), found more complicated O-isotope matrix effects in garnet where sputter rate was not correlated with the magnitude of instrumental mass fractionation. Matrix effects in carbonates are also complicated (e.g., Rollion-Bard and Marin-Carbonne, 2011; Śliwiński et al., 2016a, 2016b) although Śliwiński and colleagues were able to fit the IMF data as a function of Fe / (Fe + Mg) content of the carbonates along the dolomite – ankerite solid solution to a Hill equation, which has a similar functional form to the sigmoid that we used relating change in IMF to sputter rate in olivine.

The primary purpose of this contribution was to develop a useful calibration scheme for the accurate measurements of oxygen isotope ratios in olivine over a wide range of chemical compositions. Although the exact physics leading to matrix-dependent mass fractionation in SIMS have not been uncovered, we can nevertheless see that achieving high ionization yields by supplying more Cs at the sputtering surface may help to decrease O-isotope SIMS matrix effects. Such a strategy may provide practical benefits in improving accuracy and precision of other isotopic measurements as well.

There have been several technical approaches tried for the purpose of increasing negative secondary ionization yields for reducing matrix effects. For example, flooding the sample surface with neutral Cs has been suggested (e.g. Bernheim et al., 1979; Wirtz and Migeon, 2004) to enhance negative ion counts. Alternatively, reducing primary beam impact energy might increase useful yield (and thus reduce the matrix effect) by reducing both the sputter rate and the range (depth) of the implanted Cs. Changing the angle of incidence to be closer to normal to the sample surface (as in the CAMECA NanoSIMS) would also reduce sputter rate and improve Cs saturation, however the primary beam angle is not adjustable independent of impact energy in the CAMECA ims 1270–1290 ion microprobes. It is also worth noting that there is a practical limit to reducing sputter rates because low secondary ion intensities may prohibit use of Faraday cup detectors necessary for achieving high precision analyses.

4. Conclusions

SIMS matrix effects on instrumental mass fractionation of oxygen isotopes in olivine are reproducible between two different instruments in four different sessions and can therefore be accurately calibrated. The correlation between Fa content and instrumental mass fractionation implies that matrix effects can be corrected for in intermediate composition olivines by using a model curve and a reference IMF calibrated for a given analytical session on a primary standard (e.g., San Carlos olivine). Precision and accuracy of ~0.4‰ in δ¹⁸O is achievable at the ~10–25 μm spatial scale. Accurate knowledge of the chemical composition (Fa content) of an olivine sample is required in order to correct matrix effects.

A higher Cs concentration at the sputtered surface helps reduce SIMS oxygen isotope matrix effects. Because sputter rate is the main control on the Cs concentration in the sputtered surface for a given matrix, it may be possible in principle to develop a correction for matrix effects in IMF by comparing relative sputter rates between an unknown and a standard sample; however, measuring chemical compositions of

the samples is generally easier and more precise. For SIMS isotopic analyses of samples for which no matching mineral standards exist, one should exercise particular caution due to the potential for large matrix effects especially when very different sputter rates are found between the samples and standards.

Acknowledgements

The authors thank Frank Kyte and Rosario Esposito for assistance with EPMA. We also thank Axel Schmitt and Rita Economos for assistance with SIMS analyses. The paper has benefitted from constructive reviews by Noriko Kita and an anonymous reviewer which we appreciate. This work was supported by NASA NNX 13 AH49G and NNX 14 AJ84G (JTW), NASA NNX09AG89G (KDM), and NASA Emerging Worlds NNX15AH43G (EDY). The UCLA ion microprobe laboratory is partially supported by a grant EAR 1339051 from the NSF Instrumentation and Facilities Program.

Appendix A. Supplementary data

Supplementary data to this article can be found online at <http://dx.doi.org/10.1016/j.chemgeo.2017.03.020>.

References

- Andersen, C.A., 1970. Analytic methods for the ion microprobe mass analyzer. Part II. *Int. J. Mass Spectrom. Ion Phys.* 3, 413–428.
- Baertschi, P., 1976. Absolute ^{18}O content of standard mean ocean water. *Earth Planet. Sci. Lett.* 31, 341–344.
- Bernheim, M., Rebière, J., Slodzian, G., 1979. Negative ion emission from surfaces covered with cesium and bombarded by noble gas ions. In: *Secondary Ion Mass Spectrometry SIMS. II*. pp. 40–43.
- Chelgren, J.E., Katz, W., Deline, V.R., Evans Jr., C.A., Blattner, R.J., Williams, P., 1979. Surface cesium concentrations in cesium-ion-bombarded elemental and compound targets. *J. Vac. Sci. Technol.* 16, 324.
- Clayton, R.N., Mayeda, T.K., 1986. Oxygen isotope studies of achondrites. *Geochim. Cosmochim. Acta* 60, 1999–2017.
- Criss, R.E., 2008. Terrestrial oxygen isotope variations and their implications for planetary lithospheres. *Rev. Mineral. Geochem.* 68.
- Deline, V.R., Katz, W., Evans Jr., C.A., Williams, P., 1978. Mechanism of the SIMS matrix effect. *Appl. Phys. Lett.* 33, 832–835.
- Eiler, J.M., Graham, C., Valley, J.W., 1997. SIMS analysis of oxygen isotopes: matrix effects in complex minerals and glasses. *Chem. Geol.* 138, 221–244.
- Huberty, J.M., Kita, N.T., Kozdon, R., Heck, P.R., Fournelle, J.H., Spicuzza, M.J., Xu, H., Valley, J.W., 2010. Crystal orientation effects in $\delta^{18}\text{O}$ for magnetite and hematite by SIMS. *Chem. Geol.* 276, 269–283.
- Jogo, K., Nagashima, K., Hutcheon, I.D., Krot, A.N., Nakamura, T., 2012. Heavily metamorphosed clasts from the CV chondrite breccias Mokoia and Yamato-86009. *Meteorit. Planet. Sci.* 47, 2251–2268.
- Keil, K., 2012. Angrites, a small but diverse suite of ancient, silica-undersaturated volcanic-plutonic mafic meteorites, and the history of their parent asteroid. *Chem. Erde-Geochem.*
- Kita, N.T., Ushikubo, T., Fu, B., Valley, J.W., 2009. High precision SIMS oxygen isotope analysis and the effect of sample topography. *Chem. Geol.* 264, 43–57.
- Kita, N.T., Nagahara, H., Tachibana, S., Tomomura, S., Spicuzza, M.J., Fournelle, J.H., Valley, J.W., 2010. High precision SIMS oxygen three isotope study of chondrules in LL3 chondrites: role of ambient gas during chondrule formation. *Geochim. Cosmochim. Acta* 74, 6610–6635.
- Kolodny, Y., Bar-Matthews, M., Ayalon, A., McKeegan, K.D., 2003. A high spatial resolution $\delta^{18}\text{O}$ profile of a speleothem using an ion-microprobe. *Chem. Geol.* 197, 21–28.
- Mikouchi, T., Miyamoto, M., McKay, G., 2001. Mineralogy and petrology of the Dar al Gani 476 martian meteorite: implications for its cooling history and relationship to other shergottites. *Meteorit. Planet. Sci.* 36, 531–548.
- Nakashima, D., Kita, N.T., Ushikubo, T., Noguchi, T., Nakamura, T., Valley, J.W., 2013. Oxygen three-isotope ratios of silicate particles returned from asteroid Itokawa by the Hayabusa spacecraft: a strong link with equilibrated LL chondrites. *Earth Planet. Sci. Lett.* 379, 127–136.
- Page, F.Z., Kita, N.T., Valley, J.W., 2010. Ion microprobe analysis of oxygen isotopes in garnets of complex chemistry. *Chem. Geol.* 270, 9–19.
- Riciputi, L.R., Paterson, B.A., Ripperdan, R.L., 1998. Measurement of light stable isotope ratios by SIMS. *Int. J. Mass Spectrom.* 178, 81–112.
- Rollion-Bard, C., Marin-Carbone, J., 2011. Determination of SIMS matrix effects on oxygen isotopic compositions in carbonates. *J. Anal. At. Spectrom.* 26, 1285–1289.
- Śliwiński, M.G., Kitajima, K., Kozdon, R., Spicuzza, M.J., Fournelle, J.H., Denny, A., Valley, J.W., 2016a. Secondary ion mass spectrometry bias on isotope ratios in dolomite-ankerite, part II: $\delta^{13}\text{C}$ matrix effects. *Geostand. Geoanal. Res.* 40, 173–184.
- Śliwiński, M.G., Kitajima, K., Kozdon, R., Spicuzza, M.J., Fournelle, J.H., Denny, A., Valley, J.W., 2016b. Secondary ion mass spectrometry bias on isotope ratios in dolomite-ankerite, part I: $\delta^{18}\text{O}$ matrix effects. *Geostand. Geoanal. Res.* 40, 157–172.
- Tenner, T.J., Ushikubo, T., Kurahashi, E., Kita, N.T., Nagahara, H., 2013. Oxygen isotope systematics of chondrule phenocrysts from the CO3.0 chondrite Yamato 81020: evidence for two distinct oxygen isotope reservoirs. *Geochim. Cosmochim. Acta* 102, 226–245.
- Tenner, T.J., Nakashima, D., Ushikubo, T., Kita, N.T., Weisberg, M.K., 2015. Oxygen isotope ratios of FeO-poor chondrules in CR3 chondrites: influence of dust enrichment and H_2O during chondrule formation. *Geochim. Cosmochim. Acta* 148, 228–250.
- Treble, P.C., Schmitt, A.K., Edwards, R.L., McKeegan, K.D., Harrison, T.M., Grove, M., Cheng, H., Wang, Y.J., 2007. High resolution secondary ionisation mass spectrometry (SIMS) $\delta^{18}\text{O}$ analyses of Hulu Cave speleothem at the time of Heinrich Event 1. *Chem. Geol.* 238, 197–212.
- Valley, J.W., Kita, N.T., 2009. In situ oxygen isotope geochemistry by ion microprobe. *Mineral. Assoc. Can. Short Course* 19–63.
- Warren, P.H., Ruben, A.E., Isa, J., Gessler, N., Ahn, I., Choi, B.-G., 2014. Northwest Africa 5738: Multistage fluid-driven secondary alteration in an extraordinarily evolved eucrite. *Geochim. Cosmochim. Acta* 141, 199–227.
- Wasson, J.T., Ruben, A.E., 2003. Ubiquitous low-FeO relict grains in type II chondrules and limited overgrowths on phenocrysts following the final melting event. *Geochim. Cosmochim. Acta* 67, 2239–2250.
- Wirtz, T., Migeon, H.-N., 2004. Work function shifts and variations of ionization probabilities occurring during SIMS analyses using an in situ deposition of Cs^0 . *Surf. Sci.* 561, 200–207.
- Young, E.D., Kohl, I.E., Warren, P.H., Rubie, D.C., Jacobson, S.A., Morbidelli, A., 2016. Oxygen isotopic evidence for vigorous mixing during the Moon-forming giant impact. *Science* 351, 493–496.
- Yu, M.L., 1986. Chemical enhancement effects in SIMS analysis. *Nucl. Instrum. Methods Phys. Res. Sect. B* 15, 151–158.